7650 *Inorg. Chem.* **2009**, *48*, 7650–7658
DOI: 10.1021/ic802120n

Inorganic Chemistry
Article

Color Properties and Structural Phase Transition in Penta- And Hexacoordinate Isothiocyanato Ni(II) Compounds

T. V. Brinzari,[†] C. Tian,[‡] G. J. Halder,[§] J. L. Musfeldt,*[,†] M.-H. Whangbo,[‡] and J. A. Schlueter[§]

[†]*Department of Chemistry, University of Tennessee, Knoxville, Tennessee 37996,* [‡]*Department of Chemistry, North Carolina State University, Raleigh, North Carolina 27695-8204, and* [§]*Materials Science Division, Argonne National Laboratory, Argonne, Illinois 60439*

Received November 5, 2008

We investigated the optical properties of $(NBu_4)_3[Ni(NCS)_5]$, a pentacoordinate Ni compound, and compared the results with the more traditional hexacoordinate analogue $(NEt_4)_4[Ni(NCS)_6]$. On the basis of our complementary electronic structure calculations, the color properties of this high spin complex can be understood in terms of excitations between strongly hybridized orbitals with significant Ni d and ligand character. Variable temperature vibrational studies show mode softening with decreasing temperature and splitting near 200 K, trends that we attribute to improved low temperature intermolecular interactions and a weak structural phase transition, respectively.

I. Introduction

Materials that possess unusual coordination environments have attracted attention because of their unique geometry and uncommon chemical and physical properties that derive from such geometries.[1−4] Transition metal systems based upon Ni^{2+}, Co^{2+}, and Fe^{2+} are especially flexible, giving rise to functionalities that derive from novel bonding configurations. Work on pentacoordinate compounds established this field in the late 1950s. Some of earliest reported pentacoordinate square pyramidal Ni^{2+} complexes include low-spin compounds with polydentate ligands: $[NiX_2(triarsine)]$ and $[NiX(diarsine)_2]ClO_4$ (X = Br) as well as with monodentate ligands like $[NiX_2(HP(C_6H_5)_2)_3]$ (X = Cl, Br).[5−7] High-spin Ni^{2+} complexes such as $[X\text{-}SALen\text{-}N(C_2H_5)_2)]_2Ni$ (X = 3-Cl, 5-Cl, 3,4-benzo)(SALen = *N*,*N*′-ethylenebis(salicylideneiminate)) were reported almost a decade later and also display a square pyramidal ligand arrangement.[8] There are, however, very few systems in which Ni^{2+} is surrounded by five identical ligands. Mononuclear $[Ni(CN)_5]^{3-}$ is a unique example, in which five identical anions surround the Ni^{2+} center in a square pyramidal arrangement.[9,10] The stability of this material and of similar five-coordinate transition metal complexes with halide and pseudohalide ions can be partially explained by the presence of large trivalent cations which are able to participate in hydrogen bond formation.[11] Recently, a pentacoordinate bimetallic $[Ni_2(NCS)_8]^{4-}$ compound was discovered with pseudosquare-pyramidal and pseudotrigonal-bipyramidal environments.[12] Magnetostructural interactions were investigated in comparison to chemically similar tetra- and hexacoordinate analogues - an effective and well-known strategy.

The system of interest in this work, $[Ni(NCS)_5]^{3-}$, is a relatively rare example of a pentacoordinate Ni^{2+} complex with five chemically equivalent NCS^- ligands that co-crystallizes with organic structure-directing counterions.[13] Figure 1 displays the local Ni^{2+} environment in the pentacoordinate title compound along with that of its traditional hexacoordinate analogue $(NEt_4)_4[Ni(NCS)_6]$. The latter is similar to $(Me_4N)_4[Ni(NCS)_6]$ and $(Et_3NH)_4[Ni(NCS)_6]$ reported earlier.[14,15] Although NCS^- is considered to be less effective in stabilizing five-coordinate systems than the CN^- anion,[16]

*To whom correspondence should be addressed. E-mail: musfeldt@utk.edu.

(1) Beale, A. M.; Grandjean, D.; Kornatowski, J.; Glatzel, P.; de Groot, F. M. F.; Weckhuysen, B. M. *J. Phys. Chem. B* **2006**, *110*, 716.
(2) Xiang, H. J.; Wei, S. -H.; Whangbo, M. -H. *Phys. Rev. Lett.* **2008**, *100*, 167207.
(3) Ye, Q.; Fu, D. -W.; Tian, H.; Xiong, R. -G.; Chan, P. W. H.; Huang, S. D. *Inorg. Chem.* **2008**, *47*, 772.
(4) Okubo, T.; Kawajiri, R.; Mitani, T.; Shimoda, T. *J. Am. Chem. Soc. Comm.* **2005**, *127*, 17598.
(5) Hayter, R. G. *Inorg. Chem.* **1963**, *2*, 932.
(6) (a) Barclay, G. A.; Nyholm, R. S.; Parish, R. V. *J. Chem. Soc.* **1961**, 4433. (b) Mair, G. A; Powell, H. M.; Henn, D. E. *Proc. Chem. Soc.* **1960**, 415.
(7) Harris, C. M.; Nyholm, R. S.; Phillips, D. J. *J. Chem. Soc.* **1960**, 4379.
(8) Sacconi, L.; Nannelli, P.; Nardi, N.; Campigli, U. *Inorg. Chem.* **1965**, *4*, 943.
(9) Coleman, J. S.; Peterson, H., Jr.; Penneman, R. A. *Inorg. Chem.* **1965**, *4*, 135.
(10) Raymond, K. N.; Corfield, P. W. R.; Ibers, J. A. *Inorg. Chem.* **1968**, *7*, 1362.
(11) In general, various steric and electronic effects have to be considered as well.
(12) Larue, B.; Tran, L. -T.; Luneau, D.; Reber, C. *Can. J. Chem.* **2003**, *81*, 1168.
(13) Batten, S. R.; Murray, K. S. *Coord. Chem. Rev.* **2003**, *246*, 103.
(14) Hoffman, D. W.; Wood, J. S. *Cryst. Struct. Commun.* **1982**, *11*, 691.
(15) Kruger, P. E.; McKee, V. *Acta Crystallogr., Sect. C* **1996**, *52*, 617.
(16) Morassi, R.; Bertini, I.; Sacconi, L. *Coord. Chem. Rev.* **1973**, *11*, 343.

 Published on Web 07/10/2009 © 2009 American Chemical Society

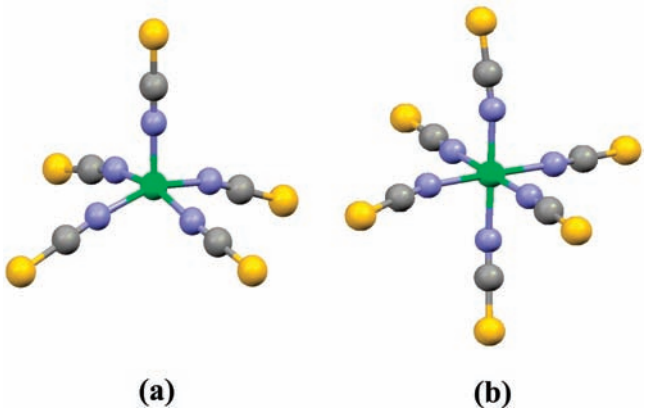

Figure 1. Local structure of the Ni^{2+}-containing chromophore for the penta- (a) and hexa-coordinate (b) compounds of interest in this work. Ni^{2+} has a high spin state in both systems. As a consequence, these building block units can form the basis for many new magnetic materials with tunable interactions.

both clusters are predicted to form based upon the 18 electron rule. Several low-spin Co^{2+} complexes have been prepared, demonstrating that NCS^- can effectively stabilize pentacoordinate complexes under certain circumstances.[17−19]

To investigate bonding in materials with non-traditional transition metal coordination environments, we measured the optical properties of $(NBu_4)_3[Ni(NCS)_5]$ and compared the results to its traditional hexacoordinate analogue. Complementary first principles electronic structure calculations were used to assign the observed excitations. We find that there is strong mixing between the metal d states and the ligands, the consequence of which is that the color band excitations show a combination of charge transfer and d to d character. The lowest energy excitation in $(NBu_4)_3[Ni(NCS)_5]$ is particularly sensitive to the local quasi-C_{4v} symmetry because the d_{z^2}-containing level relaxes significantly compared to its position in the hexacoordinate analogue with quasi-O_h symmetry. Variable temperature vibrational studies and a complementary crystallographic analysis elucidate a weak structural transition near 200 K involving local distortions in both the ligands and the organic counterions, an effect likely driven by enhanced low temperature electrostatic interactions. We conclude with a discussion of our ongoing efforts to incorporate these clusters into multifunctional hybrid materials.

II. Methods

A. Crystal Growth. $(NEt_4)_4[Ni(NCS)_6]$: Nickel thiocyanate (175 mg, 1 mmol, Alfa Aesar) was dissolved in 25 mL of water. In a separate beaker, tetraethylammonium bromide (630 mg, 3 mmol, Aldrich) and potassium thiocyanate (292 mg, 3 mmol, Aldrich) were dissolved in 10 mL of water. After these two solutions were combined, blue crystals formed over the period of a week. Anal. Calcd (%) for $C_{38}H_{80}N_{10}NiS_6$: C, 49.17; H, 8.69; N, 15.08. Found: C, 48.53; H, 8.49; N, 14.87. Mp: 176 °C.[20]

$(NBu_4)_3[Ni(NCS)_5]$: Nickel thiocyanate (175 mg, 1 mmol, Alfa Aesar) and tetrabutylammonium thiocyanate (900 mg, 3 mmol, Aldrich) were dissolved in 50 mL of hot water. Methanol (6 mL) was added to improve NBu_4^+ salt solubility. Green crystals formed upon cooling this hot solution slowly overnight. Anal. Calcd (%) for $C_{53}H_{108}N_8NiS_5$: C, 59.13; H, 10.11; N, 10.41. Found: C, 59.32; H, 10.06; N, 10.29. Mp: 106 °C.[20]

Crystallization yields were essentially quantitative as reagents were stoichiometrically mixed, and there are no byproducts associated with either reaction. Crystals were harvested when they reached an appropriate size with no specific attempts to optimize yields.

B. Structural Analysis. Crystal structures of our target compounds were determined with a Siemens SMART single crystal X-ray diffractometer equipped with a CCD-based area detector and a sealed-tube Mo Kα X-ray source with a graphite monochromator. The detector frames were integrated by use of the program SAINT[21] and the intensities corrected for absorption by Gaussian integration based on the measured crystal shape using the program XPREP of SAINT. Other systematic variations were corrected by the analysis of replicate reflections using the program SADABS.[22] The structure was solved by use of direct methods, while full-matrix least-squares refinement on F^2 (including all data) was performed, both using the program package SHELXTL.[23] The program PLATON[24,25] was used to search for higher symmetry, but none was found. A summary of the crystallographic data is provided in Table 1. Synchrotron-based powder X-ray diffraction was also carried out on the pentacoordinate material. A carefully ground polycrystalline sample of $(NBu_4)_3[Ni(NCS)_5]$ was sealed in a polyimide capillary (0.9 mm diameter). The X-rays (20.05 keV, 0.61848 Å) available at the 1-BM beamline at the Advanced Photon Source at Argonne National Laboratory were used in combination with a MAR-345 imaging plate detector to record diffraction patterns. A cryogenic system controlled temperature. The raw images were processed using Fit-2D.[26]

C. Spectroscopic Measurements. Optical transmittance experiments were carried out on single crystal and pressed pellet samples[27] over a wide energy range (25 meV−6.2 eV; 200−50,000 cm^{-1}) using a series of spectrometers including Bruker IFS 113 V Fourier transform infrared spectrometer, a Bruker Equinox 55 Fourier transform infrared spectrometer equipped with a microscope attachment, and a modified Perkin-Elmer Lambda-900 grating spectrometer. We employed 0.5 cm^{-1} resolution in the infrared and 3 nm resolution in the optical regime. Appropriate polarizers were used to separate the response along different directions for the crystalline samples. Variable temperature studies were carried out

(17) Rigo, P.; Bressan, M.; Turco, A. *Inorg. Chem.* **1968**, *7*, 1460.
(18) Boschi, T.; Nicolini, M.; Turco, A. *Coord. Chem. Rev.* **1966**, *1*, 269.
(19) Bertacco, A.; Mazzi, U.; Orio, A. A. *Inorg. Chem.* **1972**, *11*, 2547.
(20) Elemental Analyses were performed by Midwest Microlab (Indianapolis, IN).
(21) *SAINT*, Version 6.28a; Bruker AXS, Inc.: Madison, WI, 2001.
(22) Sheldrick, G. M. *SADABS*, Version 2.03a; Bruker AXS, Inc.: Madison, WI, 2001.
(23) Sheldrick, G. M. *SHELXTL*, Version 6.12; Bruker AXS Inc.: Madison, WI, 2001.
(24) Spek, A. L. *PLATON, A Multipurpose Crystallographic Tool*; Utrecht University: Utrecht, The Netherlands, 1999.
(25) Spek, A. L. *J. Appl. Crystallogr.* **2003**, *36*, 7.
(26) (a) Hammersley, A. P. ESRF Internal Report, **1997**, ESRF97HA02T. (b) Hammersley, A. P; Svensson, S. O.; Hanfland, M.; Fitch, A. N.; Hausermann, D. *High-Pressure Res.* **1996**, *14*, 235.
(27) Pellets were prepared with a 0.2% (by weight) sample concentration, using KCl as a matrix material.

Table 1. Crystal Data and Structure Refinement

	$(NEt_4)_4[Ni(NCS)_6]$		$(NBu_4)_3[Ni(NCS)_5]$	
formula	$C_{38}H_{80}N_{10}NiS_6$		$C_{53}H_{108}N_8NiS_5$	
M_W	928.19		1076.48	
cryst syst	orthorhombic		orthorhombic	
space group	*Cmca*		*Pbca*	
a/Å	18.973(2)	18.7942(12)	22.2269(8)	22.0901(9)
b/Å	21.050(3)	20.8981(15)	24.5812(9)	23.9105(10)
c/Å	38.715(5)	38.107(3)	25.0002(9)	25.0473(10)
V/Å^3	15462(6)	14966.9(18)	13659(9)	13229.6(15)
Z	12		8	
D_c/ g cm^{-3}	1.196	1.236	1.047	1.081
μ/mm^{-1}	0.655	0.677	0.472	0.488
$F(000)$	6024		4720	
R(int)	0.0582	0.0384	0.1001	0.0987
total reflns	40067	62709	99591	82414
unique reflns	8167	9461	9811	8062
$I > 2\sigma(I)$	4783	7708	4803	5161
$R(F_o)$, $R_w(F_o^2)$	0.0589, 0.1472	0.0448, 0.1089	0.0615, 0.1527	0.0510, 0.1120
T/K	298(2)	150(2)	298(2)	200(2)

$R(F_o) = \sum||F_o|-|F_c||/\sum|F_o|$; $R_w(F_o^2) = [\sum w(|F_o^2|-|F_c^2|)^2/\sum wF_o^2]^{1/2}$.

with an open flow cryostat and a temperature controller. The absorption coefficient α was calculated directly from the measured transmittance by taking into account sample thickness and loading as $\alpha = -(1/hd)\ln(T)$, where h is the loading and d is the sample thickness. Pellet data were scaled to single crystal absorption values. Standard fitting techniques and dynamics calculations (using Spartan molecular modeling software) were employed, as appropriate.

D. Electronic Structure Calculations. Spin-polarized first principles density functional theory (DFT) electronic structure calculations were carried out for isolated $[Ni(NCS)_6]^{4-}$ and $[Ni(NCS)_5]^{3-}$ units by using the Gaussian 03 code[28] with the B3LYP functional[29,30] and the 6-31G (d) basis set. To facilitate molecular orbital symmetry assignments and hence the determination of the symmetry-allowed electronic excitations, our calculations for $[Ni(NCS)_6]^{4-}$ and $[Ni(NCS)_5]^{3-}$ employed the idealized octahedral (O_h) and square pyramidal (C_{4v}) structures, respectively. These structures were constructed by using the averaged bond lengths and bond angles of the experimental structures under the constraint that each Ni−NCS unit is linear. Since the real structures of $[Ni(NCS)_6]^{4-}$ and $[Ni(NCS)_5]^{3-}$ are slightly distorted from their idealized structures, symmetry-forbidden transitions should be weakly allowed. In general, our calculations show that the orbitals of the NCS^- ligands are strongly hybridized with the orbitals of the Ni^{2+} ion, leading to both d-d and ligand−metal charge-transfer transitions.

III. Results and Discussion

A. Structure and Optical Properties of $(NEt_4)_4[Ni(NCS)_6]$. $(NEt_4)_4[Ni(NCS)_6]$ crystallizes in the orthorhombic space group *Cmca*. The structure contains two crystallographically unique Ni^{2+} centers, each with a distorted octahedral environment (Figure 1b). Ni1 lies on a mirror plane whereas Ni2 lies on a site of 2/*m* symmetry. The Ni centers are coordinated by the nitrogen atoms of six thiocyanate ligands. At 298 K, the Ni1−N bond lengths range from 2.091(4) to 2.105(5) Å, and N−Ni1−N bond angles go from 88.78(9) to 91.62(13)°. The Ni2−N bond lengths are either 2.086(3) or 2.103(5) Å, and N−Ni2−N bond angles range from 88.37(13) to 91.63(13)°. The shortest Ni−Ni separation is 11.416(1) Å.

Figure 2 displays the polarized optical absorption spectrum of $(NEt_4)_4[Ni(NCS)_6]$, the hexacoordinate model compound employed in this work. The spectrum shows three main bands at ~1.19, 1.97, and 3.2 eV with limited polarization dependence. The ratio between peak positions provides a useful criterion with which to assess local distortion from the idealized O_h structure. Here, this ratio is ~1.65 which is within the usual range for octahedral complexes, demonstrating that there is no tetragonal distortion of the Ni environment.[31]

The color properties of $(NEt_4)_4[Ni(NCS)_6]$ can be analyzed within the ligand field framework, a formalism that splits the transition metal d orbitals and their energies according to the symmetry of the surrounding ligand field as a straightforward perturbation of free ion terms. The advantage of this approach is that it provides a simple picture of symmetry and the optical excitations. The Tanabe-Sugano diagram for octahedral Ni^{2+} complexes predicts three spin-allowed transitions: $^3A_{2g}(F) \rightarrow {}^3T_{2g}(F)$, $^3A_{2g}(F) \rightarrow {}^3T_{1g}(F)$, and $^3A_{2g}(F) \rightarrow {}^3T_{1g}(P)$. Our experimentally observed peak positions are in good agreement with this picture and data for other hexacoordinate Ni^{2+} compounds.[12,32−35] One limitation of ligand field theory is that it does not allow ligands to formally mix with orbitals on the transition metal d centers. We can test the importance of metal−ligand interactions in $(NEt_4)_4[Ni(NCS)_6]$ with first principles electronic structure calculations as discussed below.

(28) Frish, M. J. et al. *Gaussian 03*, B.04; Gaussian, Inc.: Pittsburgh, PA, 2003.
(29) Becke, A. D. *Phys. Rev. A* **1988**, *38*, 3098.
(30) Lee, C.; Yang, W.; Parr, R. G. *Phys. Rev. B* **1988**, *37*, 785.
(31) .Zurowska, B.; Mrozinski, J.; Julve, M.; Lloret, F.; Maslejova, A.; Sawka-Dobrowolska, W. *Inorg. Chem.* **2002**, *41*, 1771.
(32) Forster, D.; Goodgame, D. M. L. *Inorg. Chem.* **1965**, *4*, 823.
(33) Martinez-Sanchez, J. M.; Bastida de la Calle, R.; Macias, A.; Perez-Lourido, P.; Matarranz, L. V. *Polyhedron* **2006**, *25*, 3495.
(34) Sönmez, M. *Turk. J. Chem.* **2001**, *25*, 181.
(35) Chandra, S.; Raizada, S.; Tyagi, M.; Gautam, A. *Bioinorg. Chem. Appl.* **2007**, DOI: 10.1155/2007/51483.

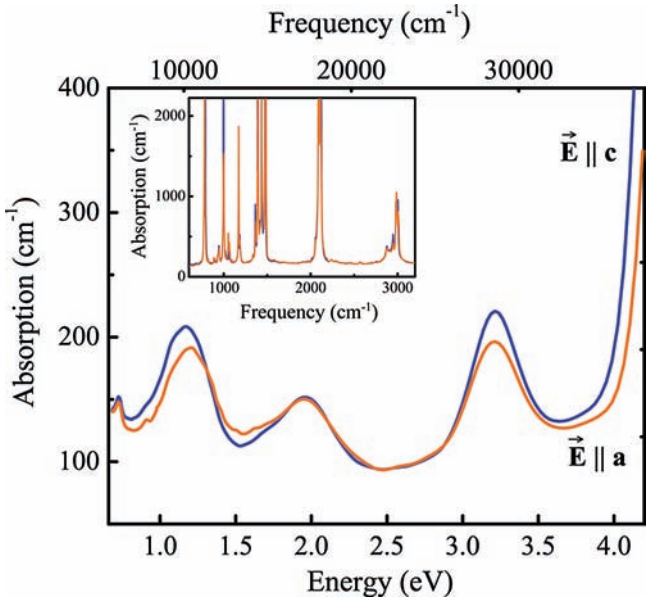

Figure 2. Polarized absorption spectrum of $(NEt_4)_4[Ni(NCS)_6]$ at room temperature. The inset shows a close-up view of the vibrational structure for light polarized along the *a* and *c* directions.

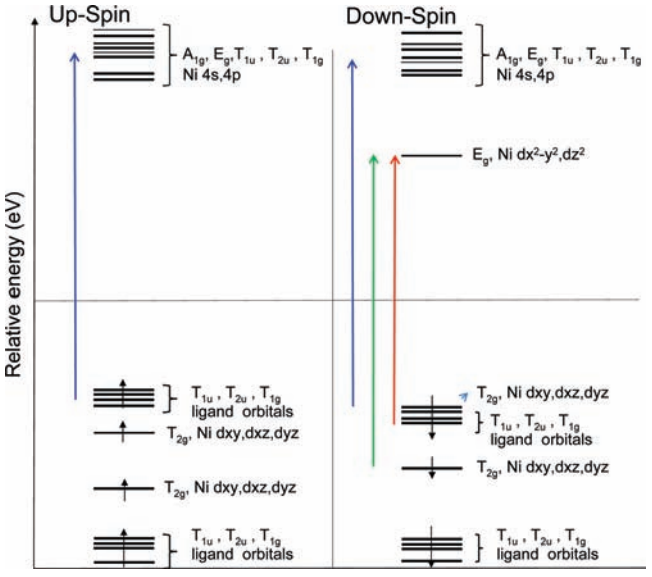

Figure 3. Electronic transitions predicted for $(NEt_4)_4[Ni(NCS)_6]$ from the DFT calculation for an isolated $[Ni(NCS)_6]^{4-}$ cluster.

The up- and down-spin levels of $[Ni(NCS)_6]^{4-}$ obtained from our DFT calculations are presented in Figure 3, where their major orbital character is also indicated. The possible electronic excitations among these levels are divided into three groups with absorption energies centered at ~5.7, 7.0, and 8.0 eV, as represented by the red, green, and blue arrows, respectively. The energy separation between adjacent groups is approximately 1 eV. Although the calculated excitation energies overestimate the experimental values, the prediction for three groups of absorption with about 1 eV energy separation is in reasonable agreement with experiment. Thus, on the basis of Figure 3, the observed absorption peaks can be interpreted as follows: the high-energy absorption peak (~3.2 eV) arises from ligand−metal charge transfer excitations, and the mid-energy peak (around 1.9 eV) from d-d excitations. This assignment is consistent with the fact that the highest-energy absorption is stronger than the mid-energy absorption. The low-energy absorption (around 1.2 eV) arises from both d-d and ligand−metal charge transfer transitions. However, some of the ligand−metal charge transfer excitations of this peak are symmetry-forbidden transitions for the idealized octahedral $[Ni(NCS)_6]^{4-}$, but should be weakly allowed in the real distorted $[Ni(NCS)_6]^{4-}$ structure. This may account for the fact that the low-energy peak shows a stronger absorption than does the mid-energy peak.

B. Structure and optical properties of $(NBu_4)_3[Ni(NCS)_5]$. $(NBu_4)_3Ni(NCS)_5$ crystallizes in an orthorhombic space group (*Pbca*) with eight distorted square pyramidal $[Ni(NCS)_5]^{3-}$ clusters. NBu_4^+ cations, which have previously been shown to act as structure directing agents,[13] control the orientation of the $[Ni(NCS)_5]^{3-}$ anions. At room temperature, there is only one crystallographically unique nickel center, which lies on a general position. The surrounding ligands form a distorted square pyramidal coordination environment with the axial ligand being slightly compressed compared with the four equatorial ligands (Figure 1a). The Ni1−N bond lengths go from 1.978(5) to 2.038(5) Å. N(ax)−Ni−N(eq) bond angles range from 98.665(192) to 101.241(187)°, and N(eq)−Ni−N(eq) bond angles range from 87.433(192) to 89.116(197)°. The basal plane nitrogen atoms lie an average of 0.041(3) out of the best plane through their centers. The transition metal center is positioned above the equatorial plane, similar to other square pyramidal Ni complexes.[10,12,36,37] The nickel atom lies 0.353(3) Å above this plane. The shortest Ni−Ni separation is 11.310(1) Å.

Following our approach for the octahedral isothiocyanato Ni^{2+} material, the color properties of square-pyramidal $(NBu_4)_3[Ni(NCS)_5]$ can be analyzed using both ligand field and molecular orbital approaches. Since distortions are relatively small, we begin by splitting the Ni^{2+} atomic terms based upon ideal C_{4v} symmetry. For a high-spin square-pyramidal complex, this analysis yields six spin-allowed transitions. Four spin-allowed transitions take place within the levels of the ^3F term ($^3B_1 \rightarrow {}^3E$, $^3A_2$, $^3B_2$, ^3E), and two occur to the ^3P term (^3E, $^3A_2$). Three of these excitations are, of course, symmetry forbidden. The position of these levels on the energy diagram is very sensitive to the $L_{ax}-Ni-L_{base}$ angle, which is about ~100° in this case.[36]

Figure 4 displays the polarized optical absorption spectrum of pentacoordinate $(NBu_4)_3[Ni(NCS)_5]$. Within the ligand field picture, we assign the three main peaks at ~0.7, 1.75, and 2.9 eV to three symmetry allowed transition from the $^3B_1$ ground state to ^3E states of the ^3F and ^3P terms, respectively. The energy values reported here are slightly different from those in other monometallic square pyramid Ni^{2+} compounds.[36,38] We attribute this difference to deviations from the idealized symmetry as well as dipole strength differences for the various ligands.[36] Within this picture, the weak feature near

(36) Ciampolini, M. *Inorg. Chem.* **1966**, *5*, 35.
(37) Orioli, P. L.; Ghilardi, C. A. *J. Chem. Soc. A* **1970**, 1511.
(38) Sacconi, L.; Orioli, P. L.; Di Vaira, M. *Chem. Commun. (London)* **1967**, *17*, 849.

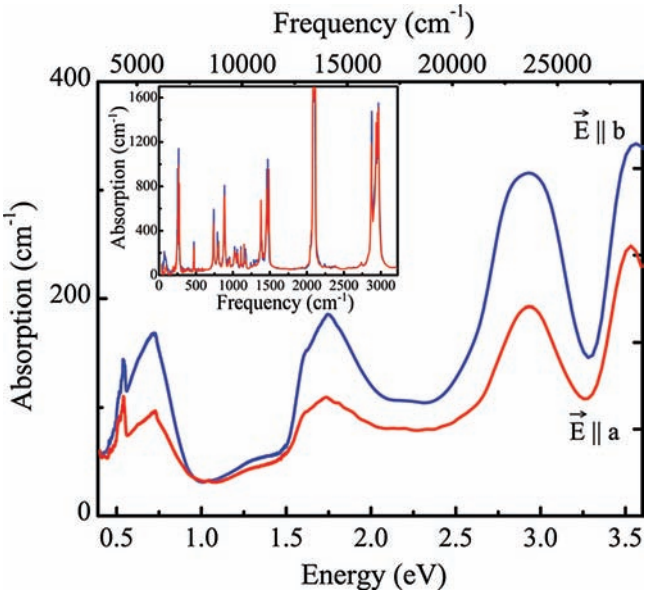

Figure 4. Absorption spectrum of $(NBu_4)_3[Ni(NCS)_5]$ at room temperature for light polarized along the *a* and *b* directions. The inset shows a close-up view of the vibrational properties, the temperature dependence of which is shown in Figure 6 and discussed in [C] **section C.**

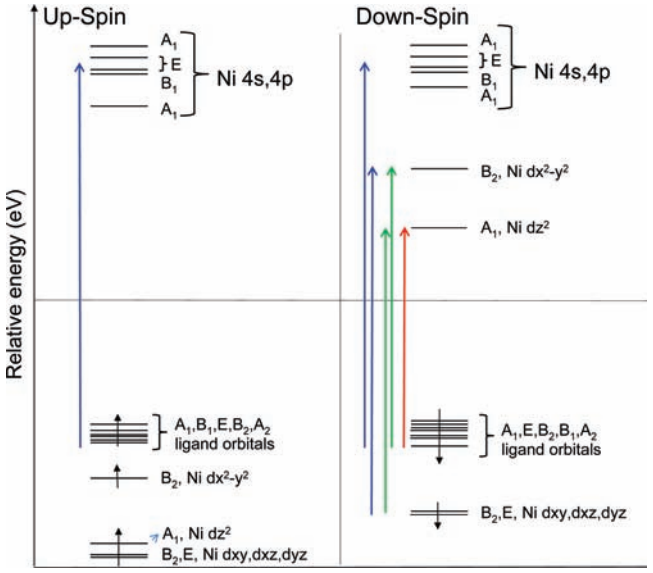

Figure 5. Possible electronic transitions predicted for $(NBu_4)_3[Ni(NCS)_5]$ from the DFT calculation for an isolated $[Ni(NCS)_5]^{3-}$ cluser.

1.28 eV is assigned as a symmetry-forbidden transition, and the 1.6 eV shoulder is assigned as a spin-flip transition to the singlet-excited ^1D state.[39,40] Interestingly, the optical properties of $(NBu_4)_3[Ni(NCS)_5]$ are in good agreement with those of pseudosquare pyramidal bimetallic $(AsPh_4)_4[Ni_2(NCS)_8]$.[12] Two additional features at 2.18 and 2.59 eV in the $[Ni_2(NCS)_8]^{4-}$ cluster are probably hidden in the spectrum of $(NBu_4)_3[Ni(NCS)_5]$ because of their low intensity.

Figure 5 shows the up- and down-spin levels of $[Ni(NCS)_5]^{3-}$, obtained from our DFT calculations, with assignment of their major orbital character. As in the case of $[Ni(NCS)_6]^{4-}$, the possible electronic excitations among the energy levels of $[Ni(NCS)_5]^{3-}$ are divided into three groups. Their absorption energies are centered around 4.2, 5.6, and 7.0 eV, as represented by the red, green, and blue arrows, respectively. The energy separation between adjacent groups is approximately 1.4 eV. Although the calculated excitation energies overestimate the experimental values, the presence of three groups of absorption with energy separation of about 1.4 eV is consistent with experiment. In terms of Figure 5, the observed absorption peaks can be interpreted as follows: the high-energy absorption peak (around 2.8 eV) arises from minority channel ligand−metal charge transfer and d-d excitations, and so does the mid-energy peak (near 1.8 eV). In contrast, the low-energy absorption (~0.7 eV) arises solely from ligand−metal charge transfer transitions.

The high-, mid-, and low-energy absorption peaks are overall lower in energy for $[Ni(NCS)_5]^{3-}$ than for $[Ni(NCS)_6]^{4-}$. Two factors are responsible for this trend. One is that the e_g level of the octahedral complex splits into the $x^2 - y^2$ and z^2 levels in the square pyramidal complex, a process that lowers the d_{z^2} level. The other is that all levels of the square pyramidal complex are lowered in energy with respect to those of the octahedral complex because of the loss of one NCS^- ligand. Thus, the change in local structure that results from ligand removal lowers excitation energies and modifies the color properties of pentacoordinate material compared to the hexacoordinate analogue.

C. Intermolecular Interactions and Structural Distortion in $(NBu_4)_3[Ni(NCS)_5]$. Various electrostatic interactions, for example hydrogen bonding, play an essential role in directing and stabilizing both local and long-range conformations in molecular materials.[41−46] They also enable significant exchange interactions in magnetic systems.[43,47−51] Although sulfur has much lower electronegativity than fluorine and oxygen, examples of hydrogen bond formation involving sulfur are well-known.[52−54]

(39) Reddy, P. P.; Reddy, Y. P. *Czech. J. Phys. B* **1978**, *28*, 1026.
(40) Holmes, O. G.; McClure, D. S. *J. Chem. Phys.* **1957**, *26*, 1686.
(41) Conner, M.; McConnell, A.; Schlueter, J.; Manson, J. *J. Low Temp. Phys.* **2006**, *142*, 273.
(42) Smith, D. M.; Woerpel, K. A. *Org. Biomol. Chem.* **2006**, *4*, 1195.
(43) Ferrer, J. R.; Lahti, P. M.; George, C.; Oliete, P.; Julier, M.; Palacio, F. *Chem. Mater.* **2001**, *13*, 2447.
(44) Oertel, C. M.; Sweeder, R. D.; Patel, S.; Downie, C. M.; DiSalvo, F. J. *Inorg. Chem.* **2005**, *44*, 2287.
(45) Mitzi, D. B. *Inorg. Chem.* **2005**, *44*, 3755.
(46) Kumai, R.; Horiuchi, S.; Sagayama, H.; Arima, T.; Watanabe, M.; Noda, Y.; Tokura, Y. *J. Am. Chem. Soc.* **2007**, *129*, 12920.
(47) Manson, J. L.; Conner, M. M.; Schlueter, J. A.; Lancaster, T.; Blundell, S. J.; Brooks, M. L.; Pratt, F. L.; Papageorgiou, T.; Bianchi, A. D.; Wosnitza, J.; Whangbo, M. -H. *Chem. Commun.* **2006**, 4894.
(48) Goddard, P. A.; Singleton, J.; Maitland, C.; Blundell, S. J.; Lancaster, T.; Baker, P. J.; McDonald, R. D.; Cox, S.; Sengupta, P.; Manson, J. L.; Funk, K. A.; Schlueter, J. A. *Phys. Rev. B* **2008**, *78*, 052408.
(49) Kajnakova, M.; Orendac, M.; Orendacova, A.; Vlcek, A.; Cernak, J.; Kravchyna, O. V.; Anders, A. G.; Balanda, M.; Park, J. -H.; Feher, A.; Meisel, M. W. *Phys. Rev. B* **2005**, *71*, 014435.
(50) Orendacova, A.; Kajnakova, M.; Cernak, J.; Park, J. -H.; Cizmar, E.; Orendac, M.; Vlcek, A.; Kravchyna, O. V.; Anders, A. G.; Feher, A.; Meisel, M. W. *Chem. Phys.* **2005**, *309*, 115.
(51) Caputo, R. E.; Willett, R. D. *Phys. Rev. B* **1976**, *13*, 3956.
(52) Steiner, T. *Acta Crystallogr., Sect. C* **1998**, *54*, 1121.
(53) Allen, F. H.; Bird, C. M.; Rowland, R. S.; Raithby, P. R. *Acta Crystallogr., Sect. B* **1997**, *53*, 680.
(54) Raj, S. S. S.; Puviarasan, K.; Velmurugan, D.; Jayanthi, G.; Fun, H. -K. *Acta Crystallogr., Sect. C* **1999**, *55*, 1318.

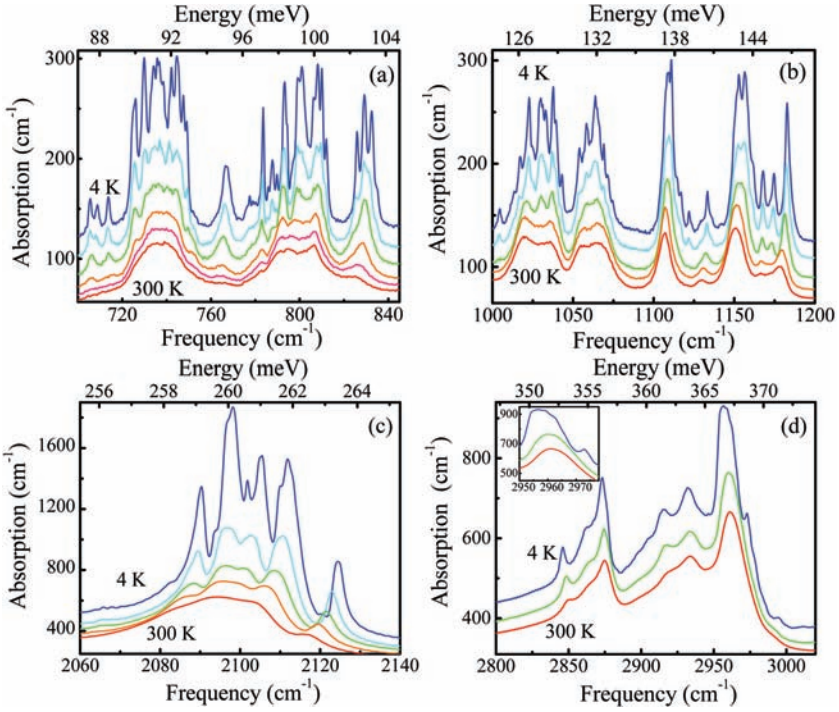

Figure 6. Close-up views of selected modes in the temperature dependent absorption spectrum of $(NBu_4)_3Ni(NCS)_5$. Panels (a) and (b) show single crystal data (E∥ b), whereas panels (c) and (d) refer to isotropic pellet data. The 4 and 300 K curves are labeled. Panel (a) displays curves at 4, 75, 125, 200, 250, and 300 K, panel (b) at 4, 75, 150, 250, and 300 K, panel (c) at 4, 100, 150, 210, and 300 K and finally panel (d) shows curves at 4, 210, and 300 K. The curves were shifted down from the 4 K results for clarity.

The ability of sulfur to engage in these interactions is, however, very dependent on the local electronic environment. For instance, Allen et al.[53] demonstrated that the acceptor abilities of sulfur in the C═S group are weak because of the modest polarity of this bond. Nevertheless, they showed that the effective electronegativity of sulfur can be increased, approaching that of the oxygen atom in a ketone if there is a substituent group *R* (e.g., amino group) in the *R*C═S linkage capable of participating in π-conjugation, thus forming an extended delocalized π-network with C═S.[53] Because of the diffuse character of the sulfur lone-pair, the C═S group remains an advantageous acceptor because it can simultaneously participate in two, three, and even four intermolecular interactions. Thus even a weak H···S interaction can contribute decisively to both local structure and overall structural stabilization. This is especially true for compounds with unusual coordination environments that are on the "knife's edge" in terms of their stability. For instance, stabilization of the bimetallic $[Ni_2Cl_8]^{4-}$ complex anion results from hydrogen bond formation between the N−H groups of the cation and the neighboring chloro ligands.[55,56] Similar bromo and iodo derivatives are not found because interactions are not as favorable.[55,56] Here we report an intermolecular electrostatic interaction between sulfur and hydrogen centers which strengthens with decreasing temperature.

Figure 6 displays close-up views of selected absorption bands of $(NBu_4)_3[Ni(NCS)_5]$ as a function of temperature. Peak assignments were carried out by comparison with chemically similar model compounds[31,32,57−59] and dynamics calculations. We assign the features at ~740 and 800 cm^{-1} to ν(NC−S) equatorial and axial stretching modes, respectively. Bands between 1000 and 1200 cm^{-1} are attributed to various $\nu(CH_2)$ bending

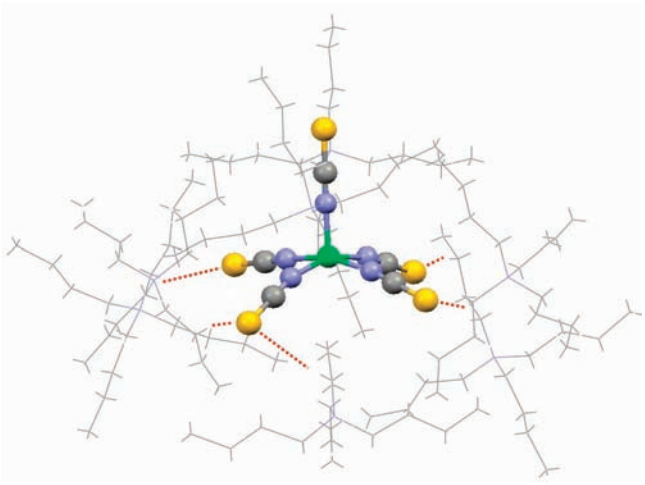

Figure 7. Intermolecular electrostatic interactions between sulfur centers in the chromophore and hydrogen centers in the organic counterions of $(NBu_4)_3[Ni(NCS)_5]$. Red dotted lines indicate near neighbor H···S interactions.

(55) Goedken, V. L.; Vallarino, L. M.; Quagliano, J. V. *J. Am. Chem. Soc.* **1970**, *92*, 303.
(56) Ross, F. K.; Stucky, G. D. *J. Am. Chem. Soc.* **1970**, *92*, 4538.
(57) Costoulas, A. J.; Werner, R. L. *Aust. J. Chem.* **1959**, *12*, 601.
(58) Ronayne, K. L.; Paulsen, H.; Höfer, A.; Dennis, A. C.; Wolny, J. A.; Chumakov, A. I.; Schünemann, V.; Winkler, H.; Spiering, H.; Bousseksou, A.; Gütlich, P.; Trautwein, A. X.; McGarvey, J. J. *Phys. Chem. Chem. Phys.* **2006**, *8*, 4685.
(59) Jones, L. H.; Badger, R. M. *J. Chem. Phys.* **1950**, *18*, 1511.

Table 2. Selected Bond Lengths (Å) for $(NEt_4)_4[Ni(NCS)_6]$ and $(NBu_4)_3[Ni(NCS)_5]$

$(NEt_4)_4[Ni(NCS)_6]$						
	298 K			150 K		
lig. no.	Ni1−N	N−C	C−S	Ni1−N	N−C	C−S
1	2.091(4)	1.149(7)	1.629(5)	2.085(2)	1.149(4)	1.649(3)
2	2.096(3)	1.133(5)	1.636(4)	2.085(2)	1.150(3)	1.643(2)
3	2.104(3)	1.145(5)	1.629(4)	2.096(2)	1.154(3)	1.645(2)
4	2.105(5)	1.127(7)	1.628(5)	2.087(3)	1.154(4)	1.641(3)
5	2.096(3)	1.133(5)	1.636(4)	2.085(2)	1.150(3)	1.643(2)
6	2.104(3)	1.145(5)	1.629(4)	2.096(2)	1.154(3)	1.645(2)
$(NEt_4)_4[Ni(NCS)_6]$						
	298 K			150 K		
lig. no.	Ni2−N	N−C	C−S	Ni2−N	N−C	C−S
1−4	2.086(3)	1.140(5)	1.632(4)	2.081(2)	1.154(3)	1.641(2)
5, 6	2.103(5)	1.146(7)	1.628(6)	2.080(3)	1.159(4)	1.642(3)
$(NBu_4)_3[Ni(NCS)_5]$						
	298 K			200 K		
lig. no.	Ni−N	N−C	C−S	Ni−N	N−C	C−S
1	1.978(5)	1.150(8)	1.616(7)	1.979(4)	1.152(6)	1.636(5)
2	2.032(5)	1.147(9)	1.619(8)	2.021(4)	1.161(7)	1.631(5)
3	2.021(5)	1.137(8)	1.617(7)	2.025(4)	1.154(6)	1.632(5)
4	2.033(5)	1.155(7)	1.623(5)	2.029(4)	1.168(6)	1.638(5)
5	2.038(5)	1.154(8)	1.628(6)	2.042(4)	1.159(6)	1.642(5)

modes. Peaks near 2100 cm^{-1} correspond to isothiocyanate stretching (ν(NC)). Those between 2800−3000 cm^{-1} are assigned as ν(CH) of the tetrabutylammonium counterion. The relatively short C−S distances (1.62 Å on average) combined with the relatively long S···H distances (2.8−3.5 Å on average) signal that hydrogen−sulfur electrostatic interactions in $(NBu_4)_3[Ni(NCS)_5]$ will be modest. In hexacoordinate $(Et_3NH)_4[Ni(NCS)_6]$, hydrogen bonding was found in the range of S···H−N distances of 2.37−2.44 Å.[15]

Vibrational spectroscopy is well-suited for the analysis of hydrogen bonding because it provides information on charge, bonding, and local structure.[60−62] One common spectroscopic signature of hydrogen bonding is mode softening.[62−64] Sometimes this effect is made manifest as a substantial change from a normal mode resonance position.[65] In other cases, variable temperature measurements can detect changes in hydrogen bonding strengths and patterns as a softening of key vibrational modes,[62−64] a trend that is quite distinct from the more common low temperature mode hardening.[66] The latter situation is observed in $(NBu_4)_3[Ni(NCS)_5]$. The data in Figure 6d reveals a 5 cm^{-1} red shift of the C−H stretching mode centered at 2960 cm^{-1} with decreasing temperature. At the same time, the position of the (NC−S) stretching modes is insensitive to temperature (Figure 6a). This suggests that improved low temperature hydrogen−sulfur interactions overcome normal low temperature hardening effects. These trends can be explained by the presence of intermolecular electrostatic interactions between sulfur centers in the ligands and hydrogen centers of the surrounding cations (Figure 7) which strengthens at low temperature.

These findings are in line with our structural results. X-ray data show an overall increase in carbon−sulfur and nitrogen−carbon bond lengths with decreasing temperature in $(NBu_4)_3[Ni(NCS)_5]$. An average increase of 0.010(5) and 0.015(4) Å was found for N−C and C−S bonds respectively upon cooling (Table 2). The NCS ligand clearly elongates at low temperature. S···H distances shorten concomitantly. The situation is similar in the hexacoordinate analogue $(NEt_4)_4[Ni(NCS)_6]$, where structural analysis shows elongation of nitrogen−carbon and carbon−sulfur bonds combined with shortened S···H distances with decreasing temperature. These details are available in CIF files in the Supporting Information.

(60) Tsvetkov, A. A.; Mena, F. P.; Loosdrecht, P. H. M.; Marel, D.; Ren, Y.; Nugroho, A. A.; Menovsky, A. A.; Elfimov, I. S.; Sawatzky, G. A. *Phys. Rev. B* **2004**, *69*, 075110.
(61) Kim, K. H.; Gu, J. Y.; Choi, H. S.; Park, G. W.; Noh, T. W. *Phys. Rev. Lett.* **1996**, *77*, 1877.
(62) Cao, J.; Haraldsen, J. T.; Brown, S.; Musfeldt, J. L.; Thompson, J. R.; Zvyagin, S.; Krzystek, J.; Whangbo, M. -H.; Nagler, S. E.; Torardi, C. C. *Phys. Rev. B* **2005**, *72*, 214421.
(63) Jones, B. R.; Varughese, P. A.; Olejniczak, I.; Pigos, J. M.; Musfeldt, J. L.; Landee, C. P.; Turnbull, M. M.; Carr, G. L. *Chem. Matter* **2001**, *13*, 2127.
(64) Brown, S.; Cao, J.; Musfeldt, J. L.; Conner, M. M.; McConnell, A. C.; Southerland, H. I.; Manson, J. L.; Schlueter, J. A.; Phillips, M. D.; Turnbull, M. M.; Landee, C. P. *Inorg. Chem.* **2007**, *46*, 8577.
(65) Toyama, A.; Hamuara, M.; Takeuchi, H. *J. Mol. Struct.* **1996**, *379*, 99.

(66) The behavior of a vibrational mode can be described as $\omega = (k/\mu)^{1/2}$, where k is the force constant of the bond and μ is the effective mass of the atoms involved in the vibration. With decreasing temperature, unit cell distances generally contract, thus increasing the size of k. As a result, mode frequencies usually increase with decreasing temperature. This effect is called "mode hardening".

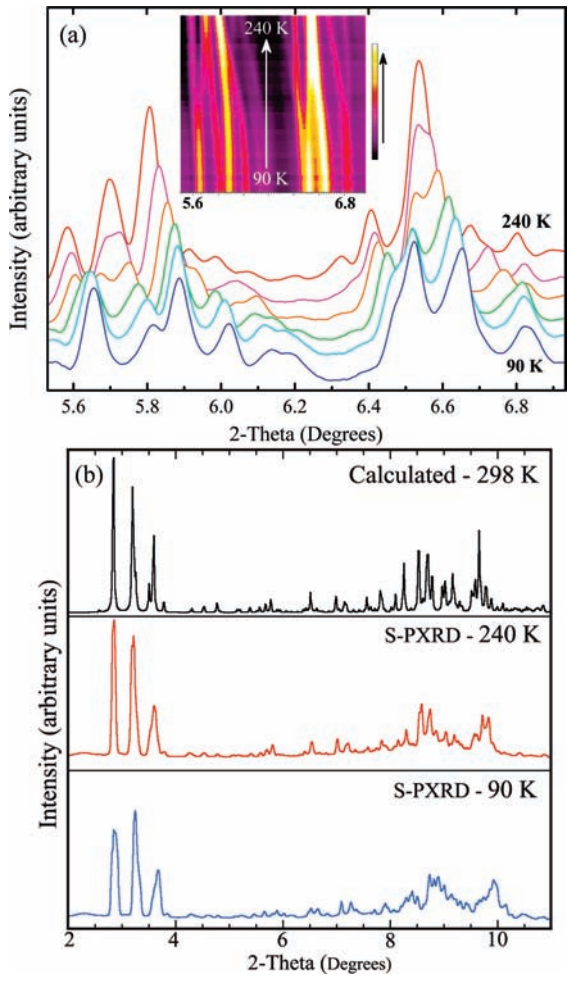

Figure 8. Synchrotron-based powder X-ray diffraction data for $(NBu_4)_3[Ni(NCS)_5]$: (a) Representative selection (5.5−7.0° 2Θ, 30 K steps) highlighting the phase transition near 200 K. (b) Comparison of calculated pattern from the single crystal refinement with patterns collected at 240 and 90 K.

Vibrational spectroscopy is also an excellent probe of local structure. It perfectly complements our X-ray results on $(NBu_4)_3[Ni(NCS)_5]$ single crystals (discussed below), the temperature range of which was limited by our ability to obtain acceptable refinements ($T \geq 200$ K). Reduction of local site symmetry and selection rule breakdown can cause (i) mode splitting and (ii) new peaks to appear.[60,64,67,68] The temperature dependence of such features can be used to detect and elucidate the nature of a structural transitions. In $(NBu_4)_3[Ni(NCS)_5]$, these effects are particularly evident in the ν(NC−S) equatorial and axial stretching modes between 740 and 800 cm^{-1} and $\nu(CH_2)$ bending modes near 1025 and 1174 cm^{-1} (Figure 6a,b). Strong symmetry breaking is observed, and new peaks arise at ∼708, 767, and 1174 cm^{-1} below 200 K. Strikingly, the new peaks are associated only with ν(NCS)- and $\nu(CH_2)$-related modes. This suggests that improved electrostatic interactions may drive the low temperature structural distortions.

The aforementioned structural transition near 200 K is supported by X-ray results. Variable temperature diffraction data reveal a subtle symmetry reduction with decreasing temperature (Figure 8). At 240 K, the observed synchrotron-based powder X-ray diffraction is consistent with the calculated pattern based on the single crystal structural refinement at 298 K, whereas significant broadening and/or splitting of the Bragg intensities is evident at 90 K. The combination of a large unit cell with relatively low symmetry and a high level of peak overlap precludes a quantitative analysis of this data.

D. Toward Multifunctional Hybrid Materials. Over the past two decades, the search for superconductivity in tetrathiafulvalene (TTF)-based cation radical salts has resulted in the exploration of a variety of thiocyanate-based diamagnetic coordination polymers, containing metals such as Cd(II), Cu(I), Hg(II), Pt(II), and Ag(I), as charge-compensating components. Among these, the κ-$(BEDT\text{-}TTF)_2Cu(NCS)_2$ salt has been highly studied because its superconducting transition temperature is among the highest in this class of materials. Here, BEDT-TTF is bis(ethylenedithio)tetrathiafulvalene. The development of magnetic cation radical salts with coexisting or interacting magnetic and conductive sublattices is of contemporary interest. Such research could lead to molecular spin-polarized conductors that have potential applications in highly efficient electroluminescent and spintronic devices. Trivalent $[M(NCS)_6]^{3-}$ (M = Cr and Fe) anions have been studied as components of such salts because of their ability to form S···S interactions between anionic and cationic components.[69,70] To our knowledge, paramagnetic analogues with divalent metals have not been investigated. Because of their moderate solubility in organic solvents, the tetraalkylammonium salts of the monomeric $Ni(NCS)_n^{m-}$ coordination complexes described in this paper provide useful electrolytes for the growth of such crystals. Through the use of these salts, we have recently crystallized the ω-$(BEDT\text{-}TTF)_2Ni(NCS)_6(EtOH)$ magnetic conductor.[71] The spectroscopic characterization of non-interacting isothiocyanato Ni(II) anions in a diamagnetic, insulating matrix of tetraalkylammonium cations described here will provide a baseline for understanding electronically coupled components in hybrid systems.

IV. Conclusion

We report the optical properties of the pentacoordinate Ni compound $(NBu_4)_3[Ni(NCS)_5]$ along with its traditional hexacoordinate analogue $(NEt_4)_4[Ni(NCS)_6]$. For both complexes, electronic structure calculations demonstrate that there is a substantial mixing of metal d and ligand orbitals of corresponding symmetry. Color properties of these materials can thus be interpreted as a combination of d-d and ligand−metal charge transfer excitations. Temperature dependent vibrational studies reveal intermolecular

(67) Choi, J.; Woodward, J. D.; Musfeldt, J. L. *Chem. Mater.* **2003**, *15*, 2797.
(68) Musfeldt, J. L.; Kamarás, J.; Tanner, D. B. *Phys. Rev. B* **1992**, *45*, 10197.
(69) Turner, S. S.; Day, P.; Gelbrich, T.; Hursthouse, M. B. *J. Solid State Chem.* **2001**, *159*, 385.
(70) Mas-Torrent, M.; Turner, S. S.; Wurst, K.; Vidal-Gancedo, J.; Veciana, J.; Day, P.; Rovira, C. *Eur. J. Inorg. Chem.* **2003**, *4*, 720.
(71) Schlueter, J. A. *unpublished results.*

electrostatic interactions between sulfur and hydrogen centers in $(NBu_4)_3[Ni(NCS)_5]$ along with a structural phase transition around 200 K that involves symmetry breaking and local distortions in the molecule. These results are supported by complementary structural studies that show reduced symmetry and elongation of C−S bonds combined with shortened S···H distances with decreasing temperature as well as changes in bond lengths and angles in the surrounding hydrogen containing cations. The competition between magnetism and superconductivity in charge transfer salts containing these $Ni(NCS)_n^{m-}$ clusters is a subject of future interest.

Acknowledgment. This work was supported by NSF DMR-0600089 (UT), MSD, BES, U.S. DoE DE-FG02-86ER45259 (NCSU) and DE-AC02-06CH11357 (ANL and APS). We thank O.A.-I. Swader for assistance in crystal indexing and P.L. Lee for beamline support.

Note Added after ASAP Publication. Due to production errors, this article was published ASAP on July 10, 2009, without all of the corrections. The corrected article was published ASAP on July 16, 2009.

Supporting Information Available: X-ray crystallographic details, including selected bond lengths and angles, in CIF format, and thermal ellipsoid plots with atom labeling. This material is available free of charge via the Internet at http://pubs.acs.org.